Journal of Molecular Modeling (2022) 28:352
https://doi.org/10.1007/s00894-022-05348-9

ORIGINAL PAPER

An investigation into the structural, electronic, and non-linear optical properties in C_N (N = 20, 24, 26, 28, 30, 32, 34, 36, and 38) fullerene cages

K. Soyarslan[1] · B. Ortatepe[1] · B. Yurduguzel[2] · M. T. Güllüoğlu[3] · Y. Erdogdu[1]

Received: 25 July 2022 / Accepted: 4 October 2022 / Published online: 12 October 2022

Abstract
The present study attempts to investigate the structural, electronic, and non-linear optical properties of C_N ($N = 20$, 24, 26, 28, 30, 32, 34, 36, and 38) fullerene cages based on Density Functional Theory (DFT). In the DFT calculations, the B3LYP/6-311G(d,p) and CAM-B3LYP/6–311 + + G(d,p) level of theories were used. The isomers of each fullerene have been received from the Fullerene Structure Library. These isomers have optimized using the B3LYP/6-311G(d,p). The results included optimization of the neutral and ionic state structures according to their multiplicity. Geometries, optimization energies, relative energies, frequencies, HOMO, LUMO, and HOMO–LUMO gap of these stable fullerene cages have been predicted by B3LYP/6-311G(d,p). Afterwards, the most stable structures have been re-optimized using the CAM-B3LYP /6–311 + + G(d,p). Finally, non-linear optical properties, Fukui functions, density of state, electron affinity, and ionization potential values of the most stable fullerene cages have been found out by the DFT/ CAM-B3LYP /6–311 + + G(d,p) level of theory. All calculation results have been compared with both C60 fullerene and the relevant literature on corresponding fullerenes.

Keywords DFT · Fullerenes · Non-linear optical properties · HOMO · LUMO energies

Introduction

Organic nanostructures such as fullerenes, nanotubes, and graphene generally receive much attention among the scholars. The main reason behind this is that organic nanostructures have properties suitable for practically various applications in different scientific fields. Among these organic nanostructures, fullerenes have outstanding properties in many different fields. With the discovery of the C_{60} fullerene by Kroto [1], an array of theoretical and experimental studies has been carried out to determine the physical and chemical properties of fullerenes, thereby characterizing a wide range of fullerenes over the years [2–4].

Currently, fullerenes find wide development application for modern science such as physics, medicine, materials science, and biology. More specifically, they have wide applications in many fields such as organic solar cells, super-capacitors, catalyzers, and superconducting materials. In addition to these properties, nano-size and thermally stable fullerenes have a wide range of applications in electronics, photonics, and nonlinear optics due to their electronic, sensing, and optical properties. The fact that fullerenes have all these application areas is due to their properties. For instance, they have a high electron affinity, unique geometric structure, electronic, and physicochemical properties. Among these properties, high electron affinity is one of its most important properties. Thanks to this property, it can have the ability to attract extra electrons and form a bound mono or poly-anion. Besides, it is nanostructures that have applications in artificial photosynthesis and photovoltaic devices [5].

✉ Y. Erdogdu
yerdogdu@gazi.edu.tr

[1] Department of Physics, Faculty of Science, Gazi University, Teknikokullar, 06500 Ankara, Turkey

[2] Programme of Electric and Energy, Kaman Technical Vocational School of Higher Education, Ahi Evran University, 40040 Kirsehir, Turkey

[3] Department of Electric and Electronic Engineering, Faculty of Engineering, Harran University, Sanliurfa, Turkey

Fullerenes, especially C60, have been an interesting research area for researchers and have been extensively studied. Today, they are an important building block for preparing materials with potential applicability in research fields such as photovoltaics, nonlinear optics, optoelectronics, and medicine [6]. Especially after the developments in C60 chemistry, it has allowed the preparation of many fullerene derivatives covalently bonded to the donor moieties. Fullerenes are used extensively in intramolecular processes such as energy and electron transfer. The C60 fullerene is known to be a particularly interesting electron acceptor in photochemical molecular devices, due to its symmetrical shape, large size, and the properties of its π-electron system [7]. They are used in the most efficient "bulk heterojunction" devices. In these devices, the fullerene derivatives are blended with conjugated semiconducting polymers. The fullerenes act as an electron acceptor to separate excitons formed when the polymer absorbs light [8].

Another important issue is analogues. The BN pair has been proposed as boron nitride analogs of the fullerenes, especially $B_{30}N_{30}$ as the analog of C_{60}. Carbon and boron nitride, being isoelectronic, tend to form similar compounds or materials. As the isoelectronic counterparts to carbon nanostructures, the boron nitrides cages and nanotubes have been extensively investigated due their high-temperature stability, low dielectric constant, large thermal conductivity, ultra-violet light emission, and oxidation resistance. The bond length, the long-order parameters, and the lattice constants are very similar between BN and C. Thus, it has been expected that the similarities should also exist between the nanoscale structures. In the present work, the analogs of C_{2X} are the BN_X (X: 10, 12, 13, 14, 15, 16, 17, 18, and 19). They could have similar structures, from one-dimensional nanotubes to three-dimensional diamond structures. Besides the similar structural features exhibited by the two species, there are also many differences between BN-made compounds and C-based compounds. For example, B and N form strong polarized covalent bonds because of the difference in their electronegativities. Therefore, BN structures have different mechanical and thermal properties. In addition to, BN nanostructures are expected to have higher reactivity than analogous carbon structures, due to the polar nature of B-N bonds. For instance, theoretical investigations predict that the BN clusters could store H_2 molecules more readily than the carbon clusters [9–14].

Despite all the theoretical and experimental studies, there are still many deficiencies in the characterization of fullerenes. So, theoretical and experimental characterization studies of fullerenes are still critical. The aim of this study is to determine the structural, electronic, and nonlinear optical properties of C_N (N=20, 24, 26, 28, 30, 32, 34, 36, and 38) fullerene cages. This study provided the theoretical calculation results of C_N fullerene cages have been presented. To the best of our knowledge, a comparative study of these fullerenes is not reported in the literature yet. To fill such a void, structural, electronic, and non-linear optical properties analyses of these fullerenes are provided in the manuscript in detail. All isomers of C_N fullerenes with various spin multiplicities were simulated by Density Functional Theory (DFT). Finally, a detailed study of the Mulliken charge, density of state, and Fukui function of these fullerenes has been presented.

Method of calculation

The researchers performed DFT calculations with Gaussian 16 code [15]. The B3LYP [16, 17], CAM-B3LYP [18] functionals were employed in the DFT calculations. The researchers used combinations of the 6-311G(d,p) [19] and 6–311 + + G(d,p) basis sets with the functionals above in the calculations.

Firstly, the isomers of all considered fullerene cages are fully optimized at B3LYP/6-311G(d,p) level of theory (abbreviated as DFT/B3LYP level) and the nature of the stationary points is checked by frequency analysis at the same computational level. The geometries of all fullerene cages were taken from the Fullerene Structure Library built by Mitsuho Yoshida [20]. Harmonic vibration frequencies at the same level were also calculated to check the stability of the geometries on the potential energy surface. Electrostatic potential maps, HOMO, and LUMO plots from results of the optimization calculations of the most stable structure of each fullerene cage were visualized with the same level.

Later, the CAM-B3LYP/6–311 + + G(d,p) (abbreviated as DFT/CAM-B3LYP level) was used on non-linear optical properties. The B3LYP method overestimated (hyper) polarizations for some large systems [18]. A new density functional Coulomb attenuated hybrid exchange correlation functional (CAM-B3LYP) has been developed and is suitable for predicting the molecular NLO properties of a large system [21–25]. This functional has been shown to provide good results for electronic excitation energies, first, second hyperpolarizabilities. Specifically, the CAM-B3LYP method was found to be suitable for calculating the hyperpolarizability of some nanotubes and nanoclusters [26]. Therefore, the CAM-B3LYP method may be a satisfactory choice to investigate the static hyperpolarizability of currently studied systems. Besides, some visualizations (Mulliken atomic charge, density of state, and Fukui function) and some calculations (ionization potentials (IP) and electron affinities (EA) and the vertical detachment energy (VDE) calculations) were performed by CAM-B3LYP methods.

Since IP and EA are essential properties that reflect the stability of fullerene cages, IP and EA were calculated from the optimization energies of the most stable geometries of neutral and charged fullerene cages [27]. The IP

was obtained by considering the difference between the optimized energies of the neutral fullerene cages and their cations. In this study, the researchers evaluated the IP versus fullerene cage size.

$$IP = E(optimized\ cation) - E(optimized\ neutral) \quad (1)$$

EA is defined as the energy obtained when an electron is added to the isolated atom. Adiabatic electron affinity (EA_{ad}) values for the lowest energy isomers of fullerene cages were computed in this study. The EA_{ad} is defined as the optimization energy difference in the most stable neutral and anion state [27].

$$EA_{ad} = E(\text{optimized neutral}) - E(\text{optimized anion}) \quad (2)$$

The vertical electron affinity (EA_{vert}) is the energy difference between the optimized neutral state and the anionic state without changing the geometry in the neutral state [27].

$$EA_{vert} = E(rmoptimized\ neutral) - E(anion\ at\ optimized\ neutral\ geometry) \quad (3)$$

The vertical detachment energy (VDE) is the energy required to remove an electron from the anionic fullerene cages without changing its geometry. As understood from the definition, it is regarded as the energy difference between the neutral state without changing the geometry in the optimized anionic state and the optimized anion state [27].

$$\text{VDE} = E(\text{neutral at optimized anion geometry}) - \text{E(optimized anion)} \quad (4)$$

It is important to determine the nonlinear optical properties of fullerenes. Theoretically, making (hyper)polarizability calculations might provide data for future studies of fullerenes. The energy of a system in the weak and homogeneous electric field can be defined as:

$$E = E^0 - \mu_\alpha F_\alpha - \frac{1}{2}\alpha_{\alpha\beta}F_\alpha F_\beta - \frac{1}{6}\beta_{\alpha\beta\gamma}F_\alpha F_\beta F_\gamma - \ldots \quad (5)$$

where E^0 is the total molecular energy in the absence of an electric field. F_α is the electric field component along the α direction. The μ_α, $\alpha_{\alpha\beta}$, and $\beta_{\alpha\beta\gamma}$ denote dipole moment, polarizability, and the first-order hyperpolarizability respectively [28]. The dipole moment (μ), the mean polarizability ($\overline{\alpha}$), the anisotropy of the polarizability ($\Delta\alpha$), and the first-order hyperpolarizability (β_0) are defined as:

$$\mu^2 = \mu_x^2 + \mu_y^2 + \mu_z^2 \quad (6)$$

$$\overline{\alpha} = \left(\alpha_{xx} + \alpha_{yy} + \alpha_{zz}\right)/3 \quad (7)$$

$$\Delta\alpha = \frac{1}{\sqrt{2}}\left[\left(\alpha_{xx} - \alpha_{yy}\right)^2 + \left(\alpha_{yy} - \alpha_{zz}\right)^2 + \left(\alpha_{zz} - \alpha_{xx}\right)^2 + 6\left(\alpha_{xy}^2 + \alpha_{yz}^2 + \alpha_{xz}^2\right)\right]^{1/2} \quad (8)$$

$$\beta_x = \beta_{xxx} + \beta_{xyy} + \beta_{xzz} \quad (9)$$

$$\beta_y = \beta_{yyy} + \beta_{yzz} + \beta_{yxx} \quad (10)$$

$$\beta_z = \beta_{zzz} + \beta_{zxx} + \beta_{zyy} \quad (11)$$

$$\beta_0 = \left[\left(\beta_{xxx} + \beta_{xyy} + \beta_{xzz}\right)^2 + \left(\beta_{yyy} + \beta_{xxy} + \beta_{yzz}\right)^2 + \left(\beta_{zzz} + \beta_{xxz} + \beta_{yyz}\right)^2\right]^{1/2} \quad (12)$$

In general, the main purpose of molecular electrostatic potential (MEP) maps is to explain the charge distribution of the working system. In this calculation, a map was created due to the properties of the nucleus and the nature of the electrostatic potential energy. These visualizations were used to illustrate concepts such as polarity, electronegativity, and similar properties. These maps were sampled over the entire accessible surface of the studied structure. The three-dimensional isosurfaces of MEPs showed electrostatic potentials superimposed on a surface of electron density. The most negative electrostatic potential was shown in red while the most positive electrostatic potential was presented in blue [29].

Fukui function is an important concept in conceptual DFT, and it has been widely used in prediction of reactive site. It is also used as a descriptor in quantitative structure–activity relationships. It calculated with the help of the following equations. In these equations, q_k is the atomic charge at the r_{th} atomic site. The N, N + 1, and N − 1 impressions show neutral, anionic, and cationic states, respectively. [29].

$$f_k^+ = q_k(N+1) - q_k(N) \text{ for nucleophilic attack} \quad (13)$$

$$f_k^- = q_k(N) - q_k(N-1) \text{ for electrophilic attack} \quad (14)$$

$$f_k^0 = \frac{1}{2}\left[q_k(N+1) - q_k(N-1)\right] \text{ for neutral (radical) attack} \quad (15)$$

Euler's theorem [30] provides a rule for pentagonal and hexagonal numbers for C_{20} cage fullerene and fullerenes with an even number of atoms greater than C_{20} cage. C_{nm} ($n \geq 2$; m: even numbers) fullerene cages have twelve pentagons. The number of hexagons was determined by the expression ($n/2 - 10$). Pentagonal and hexagonal numbers were given in the correspond table for each fullerene.

Results and discussions

The present study investigates the structural, electronic, and non-linear optical properties of neutral, cationic (single positive charge), and anionic (single negative charge) fullerenes. Geometry optimization of the neutral and charged states with different spin multiplicities was carried out for each of the fullerenes. The lowest-energy structures of these fullerenes were shown in Figs. 1–9. Pentagon/hexagon numbers,

symmetry, the optimized energies, and relative energies of all isomer of the fullerene cages with various spin multiplicities were given in Tables S1-S9. The results were discussed in the following sections.

C_{2N} (N:0, 4, 6, and 8) fullerenes

Fullerenes are closed-cage carbon structures consisting of 12 pentagons and certain number of hexagons. For each fullerene, the possible hexagon numbers could be 0, 2, 3, 4, 5, and more. The structure consisting of 12 pentagons without hexagons is the smallest possible fullerene. Thus, the smallest theoretically possible fullerene is C_{20}. The C_{20} with a dodecahedral cage structure is regarded as the smallest fullerene existing. It only comprises 12 pentagons and 30 bonds. Kroto [1] expressed the pentagon isolation rule, which stipulates that the most stable fullerenes should have 12 pentagons and that these pentagons should be as far apart as possible. Considering this rule, the C_{20} fullerene cage should be highly unstable. It is sometimes called "unconventional fullerene."

The structure of the C_{20} fullerene cage has I_h symmetry. Besides, the C_{20} fullerene cage also has eight structures with subgroup symmetry. Wang [31] et al. reported that a symmetry path from I_h symmetry to C_1 symmetry found for C_{20} fullerene cage. Based on this result, the structure with D_{2h} symmetry is the most stable in this path. The researchers took Wang's suggestion for the C_{20} as a starting point. However, negative frequency was detected in the structure's calculation with D_{2h} symmetry. Therefore, the calculations were continued with the structure with D_2 symmetry. It is structurally very similar between the structure with D_2 symmetry and the structure with D_{2h} symmetry. The researchers have done all the following calculations for the C_{20} fullerene cage with geometry D_2. Table S1 presented all calculation results such as optimization energy for each multiplicity, symmetry, and geometry. The results showed that the most stable state of C_{20} fullerene obtained the singlet spin multiplicity for neutral state and quartet spin multiplicity for ionic cases. Figure 1 demonstrated the optimized geometry (a), Mulliken charge distribution (b), MEP counter (c), and HOMO–LUMO plot (d) of the most stable isomer of the C_{20} fullerene cage.

As seen in Fig. 1, the distribution of Mulliken charges was formed as 0.433 a.u. (eight atoms in green color), – 0.409 a.u. (four red atoms on the top and bottom), -0.312 a.u. (four red atoms on the side edges), and -0.143 a.u. (four atoms in dark red color). Figure 1 shows the gaps between the highest occupied molecular orbital (HOMO) and the lowest unoccupied molecular orbital (LUMO) plots. The researchers calculated at -5.442 eV (HOMO energy), -3.506 eV (LUMO energy), and 1.937 eV (HOMO–LUMO gap energy) by DFT/B3LYP level.

Prinzbach [32] et al. accomplished the first synthesis of C_{20}. In their study, $C_{20}H_{20}$ was firstly converted to $C_{20}Br_{20}$ by substitution of H atoms with Br atoms. Then, $C_{20}Br_{20}$ was debrominated to synthesize C_{20} fullerene. Apart from this study, many studies have been carried out on the synthesis of C_{20} [33]. Prinzbach [32] et al. reported that the C_{20} fullerene had an EA of 2.25 eV by its photoelectron spectrum. In other studies on EA of the C_{20} fullerene cage, this value was determined as 2.7 eV by Yang [34] et al., 2.65 eV by Wang [35] et al., and 2.689 eV by Wang [36] et al. According to the results from the present calculations, 2.391 eV was predicted as EA of C_{20} fullerene cage by DFT/CAM-B3LYP level (Table 1). The C_{20} fullerene cage has a very symmetrical structure. As seen in Table 1, the μ and β_0 components of the C_{20} fullerene cage are all zero. However, the C_{20} fullerene has relatively small polarizability. The $\overline{\alpha}$ and the $\Delta\alpha$ were predicted at 27.59×10^{-24} esu and 1.552×10^{-24} esu by DFT/CAM-B3LYP level, respectively.

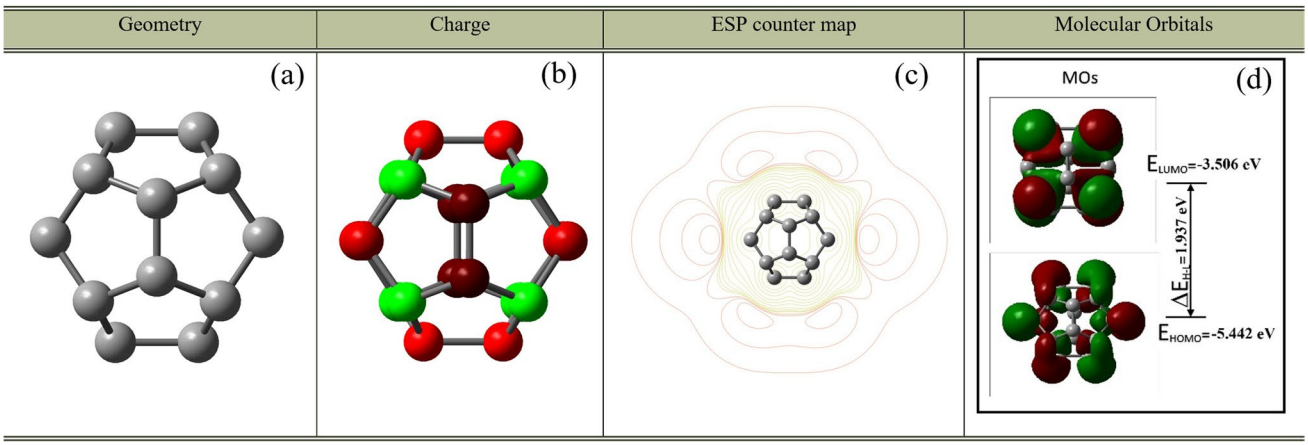

Fig. 1 Geometry, Mulliken charge, ESP counter map and HOMO, and LUMO plots of C20 fullerene cage

Table 2S provides all calculation results such as optimization energy for each multiplicity, symmetry, and geometry for C_{24} fullerene cage. Considering the optimized geometry in Table S2, C_{24} fullerene cage comprises two hexagons at the top and bottom, and 12 pentagons at the waist. Because the first member of the fullerene cage family having a magic number is the C_{24} fullerene cage, Kroto suggested that fullerenes Cn with magic numbers (*n*: 24, 28, 32, 36, 50, 60, and 70) should have enhanced stability relative to those with similar numbers of atoms [1]. The fullerene possesses ideal D_{6d} symmetry [37]. As a starting point of the study, the C_{24} fullerene cage with D_{6d} symmetry was optimized. However, negative frequency was obtained in the structure's calculation with D_{6D} symmetry. Jensen [37] et al. noted that this structure with D_{6d} symmetry is stable geometry. Nevertheless, it was found that C_{24} fullerene cage with D_{6d} was in the transition structure in the calculations made on $D_{H(D)}$ and 6-31G (d) basis sets. Similarly, it was determined that C_{24} fullerene cage with D_{6d} was in a transition structure in the present studies. Hence, the C_{24} symmetry was reduced from D_{6d} to D_6 symmetry. The C_{24} fullerene cage with D_{6d} and its D_6 symmetric structure were very similar structurally. In that symmetry, C_{24} fullerene cage with D_6 was the most stable. The researchers noted that the most stable state of C_{24} fullerene cage determined the singlet spin multiplicity for neutral state, doublet spin multiplicity for anionic case, and quartet spin multiplicity for cationic case. Figure 2 showed the optimized geometry (a), Mulliken charge distribution (b), MEP counter (c), and HOMO–LUMO plot (d) of the most stable isomer of the C_{24} fullerene cage.

As seen in Fig. 2, the Mulliken charge of the atoms shown in red color is -0.148 a.u., and the charge of atoms shown in green color is 0.148 a.u. by DFT/CAM-B3LYP level. If the Mulliken charge distribution is examined, it could be seen that two different charges are distributed symmetrically. The researchers calculated at − 6.050 eV (HOMO energy), − 4.221 eV (LUMO energy), and 1.829 eV (HOMO–LUMO gap energy) by DFT/B3LYP level.

Janjanpour [38] et al. reported that the EA and IP of the C_{24} fullerene cage were predicted at 7.47 eV and 2.98 eV by B3LYP/6–31 + G (d). In the present study, the computed IP, $EA_{ad,}$ and VDE values were obtained at 7.691 eV, 3.252 eV, and 2.699 eV by means of DFT/CAM-B3LYP, respectively (Table 1). The results showed that C_{24} fullerene cage obtained a great EA_{vert} value at 3.091 eV by DFT/CAM-B3LYP level. It indicated that C_{24} fullerene cage was a great electron acceptor.

The most stable geometry of the C_{24} fullerene cage possesses D_6 symmetry group. Given this structure, it could be stated that C_{24} had a very symmetrical structure. So, μ and β_0 components of the C_{24} fullerene cage were all zero. Kosar [39] et al. reported that $\overline{\alpha}$ of the C_{24} fullerene cage theoretically obtained 31.863×10^{-24} esu (215 a.u.) by B3LYP/6–31 + G(d) level. In the present study, $\overline{\alpha}$ and $\Delta\alpha$ were predicted at 32.04×10^{-24} esu, and 8.242×10^{-24} esu by DFT/CAM-B3LYP level (Table 2).

Table 1 Ionization potentials, electron affinities, vertical electron affinity, and vertical detachment energy of C_N and C_M fullerene cage by CAM-B3LYP/6–311 + + G(d,p)

	C_{20}	C_{24}	C_{26}	C_{28}	C_{30}	C_{32}	C_{34}	C_{36}	C_{38}
IP*	7.142	7.691	7.443	8.349	7.808	8.178	7.450	7.335	7.278
EA_{ad}*	2.391	3.252	2.618	2.864	3.559	3.025	2.955	2.889	2.957
EA_{vert}*	2.089	3.091	2.452	2.733	3.385	2.769	3.062	2.815	2.775
VDE*	2.699	3.572	2.815	3.007	3.689	3.305	3.163	2.962	3.143

*All values are in eV units

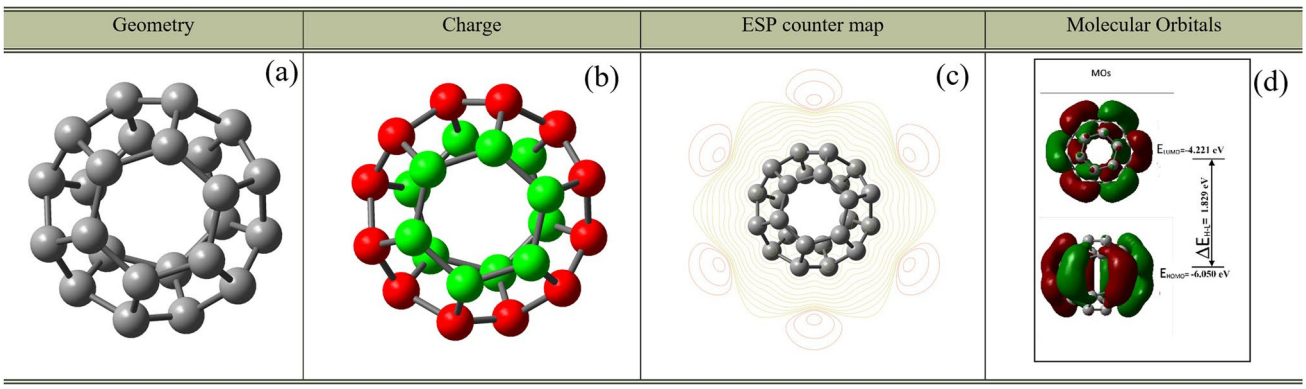

Fig. 2 Geometry, Mulliken charge, ESP counter map and HOMO, and LUMO plots of C24 fullerene cage

The following closed fullerene cage by size is C_{26}, of which there is only one classical closed-cage isomer. The highest possible symmetry of C_{26} is D_{3h}. The C_{26} fullerene cage comprises three consecutively connected hexagons and 12 pentagons. A ring is formed by connecting hexagons. Pentagons have a structure that could form bridges to these rings. Table S3 provides all calculation results such as optimization energy for each multiplicity, symmetry, and geometry for C_{26} fullerene cage. The researchers could not get a negative frequency in the frequency calculations of this fullerene cage. The results indicated that the most stable state of C_{26} fullerene cage determined the quintet spin multiplicity for neutral state, quartet spin multiplicity for anionic case, and sextet spin multiplicity for cationic case. Figure 3 showed the optimized geometry (a), Mulliken charge distribution (b), MEP counter (c), and HOMO–LUMO plot (d) of the most stable isomer of the C_{26} fullerene cage.

As seen in Fig. 3, the Mulliken atomic charges on C in the C_{26} fullerene cage were divided into four groups: − 0.145 a.u. (six atoms in dark red color), 0.290 a.u. (twelve atoms in green color), − 0.434 a.u. (six atoms in red color), and − 0.001 a.u. (two atoms in black color). Balevicius [40] et al. put forth that the HOMO and LUMO energies of C_{26} fullerene cage were determined at − 8.6 1 eV and − 4.64 eV, respectively. Because the most stable state of C_{26} fullerene cage determined the quintet spin multiplicity for neutral state, HOMO and LUMO of C_{26} fullerene cage could be designated as α and β orbitals. The researchers calculated − 6.135 eV (HOMO energy of the α orbital) and − 2.927 eV (LUMO energy of the α orbital), − 5.929 eV (HOMO energy of the β orbital), and − 4.314 eV (HOMO energy of the β orbital).

To gain insight into the electronic properties of the lowest energy isomer, we evaluated the IP, EA, and VDE of C_{26} fullerene cage at the DFT/CAM-B3LYP level (Table 1). In the present study, the researchers obtained at 7.443 eV (IP), 2.618 eV, 2.452 eV (adiabatic and vertical EA), and 2.815 eV (Vertical detachment energy). Janjanpour [38] et al. reported that the IP and EA in the C_{26} fullerene cage were predicted at 2.95 eV and 3.34 eV by B3LYP/6–31 + G (d), respectively. An [41] et al. argued that the EA_{vert} of the most stable geometry of C_{26} fullerene cage were 2.72 eV.

Table 2 Dipole moment (Debye), the mean polarizability ($\overline{\alpha}$), the anisotropy of the polarizability ($\Delta\alpha$), and the mean first-order hyperpolarizability (β_0) of neutral C_N and C_M fullerene cages by CAM-B3LYP/6–311 + + G(d,p)

	C_{20}	C_{24}	C_{26}	C_{28}	C_{30}	C_{32}	C_{34}	C_{36}	C_{38}
μ*	0.000	0.000	0.000	0.000	0.119	0.000	0.113	0.000	0.033
$\overline{\alpha}$**	27.59	32.04	34.14	35.99	40.15	43.43	46.06	47.56	49.95
$\Delta\alpha$ **	1.552	8.242	5.588	0.000	5.438	8.035	8.103	0.909	5.917
β_x***	0.000	0.000	0.000	0.000	− 0.600	0.000	0.000	0.000	0.000
β_y***	0.000	0.000	0.000	0.000	− 1.289	0.000	0.000	0.000	0.000
β_z***	0.000	0.000	0.000	0.000	− 1.493	0.000	− 2.656	0.000	− 0.289
β_0***	0.000	0.000	0.000	0.000	2.062	0.000	2.656	0.000	0.289

*The dipole moment is in Debye units

**The mean polarizability, the anisotropy of the polarizability is in (10^{-24}) esu units. (1 a.u. = 0.1482×10^{-24} esu)

***The mean first order hyperpolarizability is in (10^{-30}) esu units. (1 a.u. = 8.6393×10^{-33} esu)

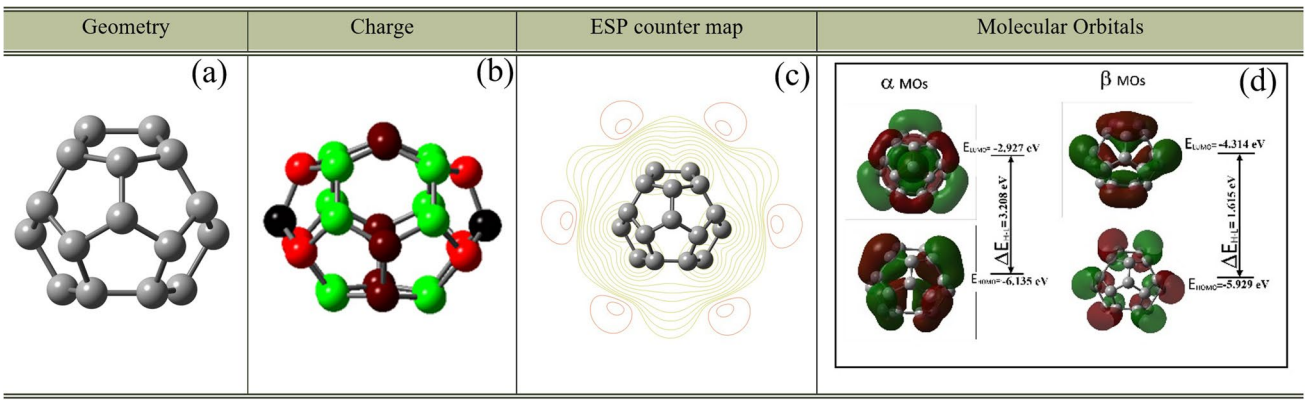

Fig. 3 Geometry, Mulliken charge, ESP counter map and HOMO, and LUMO plots of C26 fullerene cage

The most stable geometry of the C_{26} fullerene cage possesses D_{3h} symmetry group. Regarding this structure, it could be stated that C_{26} had a very symmetrical structure. So, μ and β_0 components of the C_{26} fullerene cage were all zero. The $\overline{\alpha}$ of C_{26} fullerene cage was calculated as 34.14×10^{-24} esu and the $\Delta\alpha$ of C_{26} fullerene cage was calculated to be $5.588\times10-^{24}$ esu by DFT/CAM-B3LYP level (Table 2).

C_{28} fullerene plays an important role in theoretical studies on fullerenes smaller than C_{30}. C28 are one of the magic-number small fullerenes The researchers reported that the C_{28} had two isomers with T_d and D_2 symmetry [42]. The researchers optimized the two isomer with different spin states to achieve the most stable geometry. According to the results of the optimization calculations, the isomer of T_d symmetry of the C_{28} fullerene cage had the most stable isomer. The C_{28} fullerene cage comprises 4 hexagons and 12 pentagons. The C_{28} has been reported to have a tetrahedral structure, in which there are three isolated pentagons, one at each corner, which are not directly fused. In the isomer with T_d symmetry, the researchers reported that the most stable state of C_{28} fullerene cage determined the quintet spin multiplicity for neutral state and quartet spin multiplicities for ionic cases. The researchers could not get negative frequency in the frequency calculations of this structure. Table S4 presents all calculation results such as optimization energy for each multiplicity, symmetry, and geometry for C_{28} fullerene cage. Figure 4 demonstrated the optimized geometry (a), Mulliken charge distribution (b), MEP counter (c), and HOMO–LUMO plot (d) of the most stable isomer of the C_{28} fullerene cage.

As seen in Fig. 4, the Mulliken atomic charges on C in the C_{28} fullerene cage were divided into three groups: 0.318 a.u. (twelve atoms in green color), – 0.109 a.u. (twelve atoms in dark red color), and – 0.627 a.u. (four atoms in red color). The HOMO–LUMO gap of the neutral C_{28} fullerene cage with Td symmetry was predicted at 4.201 eV for alpha orbital and 2.321 eV for beta molecular orbital by DFT/B3LYP level. These values were quite large when compared to the values of those of C_{60} and C_{70} fullerene cages.

Castro [43] et al. have put forward that the IP and EA for C_{28} fullerene cage would contribute to the understanding of its behavior in electron detachment and electron affinity situations. The calculated IP and EA_{Ad} were obtained as 7.69 eV and 3.39 eV. The results of the present study showed that 8.349 eV and 2.864 eV values were determined as IP and EA_{Ad} by DFT/CAM-B3LYP level. EA_{vert} were obtained at 2.733 eV and 3.007 eV for VDE by DFT/CAM-B3LYP level (Table 1).

In the present study, the researchers calculated the $\overline{\alpha}$ of C_{28} fullerene cage as 35.99×10^{-24} esu. The researchers note it is consistent with the value 40.44×10^{-24} esu calculated by Sabirov et al. [44]. Since C_{28} fullerene cage has a high symmetry (T_d symmetry), all components of the μ and β_0 values are found as zero (Table 2).

C_{3N} (N:0, 2, 4, 6, and 8) fullerenes

Based on the DFT calculation results, three C_{30} isomers were theoretically differentiated by D_{5h}-I-C_{30} isomer, C_{2v}-II-C_{30} isomer, and C_{2v}-III-C_{30} isomer. Table S5 provides all calculation results such as optimization energy for each multiplicity, symmetry, and geometry for C_{30} fullerene cages. Accordingly, the ground state C_{2v}-II-C_{30} isomer with singlet multiplicity was more stable than C_{2v}-I-C_{30} and D_{5h}-I-C_{30} isomers. The relative energy of C_{2v}-I-C_{30} and D_{5h}-I-C_{30} isomers determined as 28 kcal mol^{-1} and 55.81 kcal mol^{-1}. The C_{30} cage comprises 5 hexagons and 12 pentagons. The researchers could not get negative frequency in the frequency calculations of this structure. The most stable state of the cationic and anionic C_{2v}-II-C_{30} isomer obtained doublet spin multiplicity. Figure 5 showed the optimized geometry (a), Mulliken charge distribution (b), MEP counter (c), and HOMO–LUMO plot (d) of the most stable isomer of the C_{30} fullerene cage.

As seen in Fig. 5, the Mulliken atomic charges on C in the C_{30} fullerene cage were divided into ten groups. The three groups have positive Mulliken charges of 0.289 a.u., 0.188 a.u., and 0.183 a.u., and their colors on six atoms appear

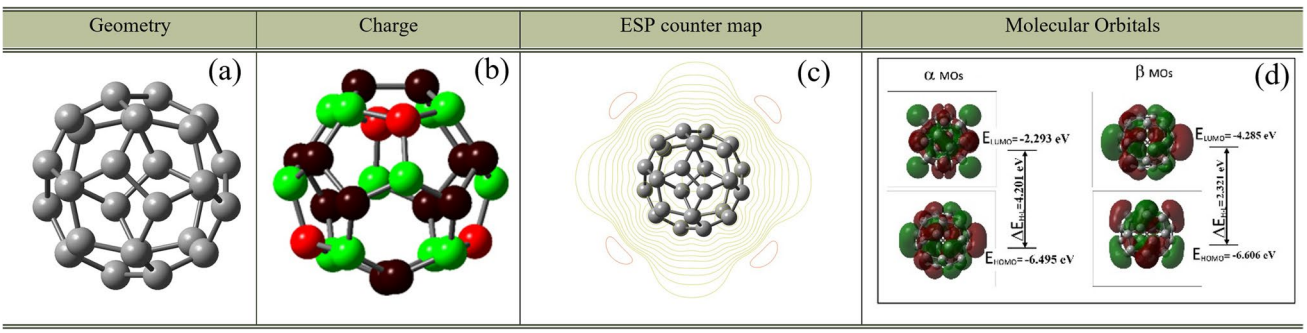

Fig. 4 Geometry, Mulliken charge, ESP cour map and HOMO, and LUMO plots of C28 fullerene cage

as green color and its shades. The three positively charged groups have a charge of 0.029 a.u., 0.008 a.u., and 0.001 a.u., and their colors on eleven atoms appear in dark green color and its shades. The two groups have negative Mulliken charges of − 0.251 a.u. and − 0.195 a.u., and their colors on four atoms appear as red color and its shades. The three negatively charged groups have a charge of − 0.078 a.u. and ⁻0.068 a.u., and their colors on eight atoms appear in dark red color and its shades.

Paul [5] et al. argued that 7.352 eV and 2.761 eV values were obtained as IP and EA by ωB97XD functional with 6–311 + G (d, p) basis set, respectively. In the present study, these properties were calculated at 7.808 eV for IP and 3.559 eV for EA_{ad} by DFT/CAM-B3LYP level. Moreover, 3.385 eV and 3.689 eV were determined as EA_{vert} and VDE, respectively (Table 1). Paul et al. [5] reported that the μ of C30 fullerene cage was calculated at 0.12 Debye by B3LYP functional with 6–311 + G (d, p) basis set. In the present study, this value was predicted at 0.119 Debye by DFT/CAM-B3LYP level. In the same study of Paul et al. [5], $\overline{\alpha}$ value of C30 fullerene cage was calculated as 43.79×10^{-24} esu, and this value was determined as 40.151×10^{-24} esu in the present study. Similarly, while the $\Delta\alpha$ value of C_{30} fullerene cage was determined as 17.64×10^{-24} esu by Paul et al. [5], it was determined as 5.438×10^{-24} esu in the present study. The β_0 value of C_{30} fullerene cage was obtained at 0.76×10^{-30} esu (CAM-B3LYP/6–311 + G(d,p)) by Paul et al. [5] In the present study, this value was predicted as 2.062×10^{-30} esu (DFT/CAM-B3LYP) (Table 2).

The C_{32} fullerene cage had six isomers. These isomers were named as D_3-VI-C_{32}, C_2-IV-C_{32}, C_2-I-C_{32}, D_2-II-C_{32}, D_{3d}-III-C_{32}, and D_{3h}-V-C_{32} fullerene cages. Table S6 presents all calculation results such as optimization energy for each multiplicity, symmetry, and geometry for C_{32} fullerene cages. According to DFT results, D_3-VI-C_{32} fullerene cage with singlet multiplicity was the most stable among the C_2-IV-C_{32}, C_2-I-C_{32}, D_2-II-C_{32}, D_{3d}-III-C_{32}, and D_{3h}-V-C_{32} fullerene cages. Relative energies of the all C_{32} fullerene cages reported 25.74 kcal mol^{-1} (C_2-IV-C_{32}), 54.59 kcal mol^{-1} (C_2-I-C_{32}), 65.59 kcal mol^{--1} (D_2 -II-C_{32}), 74.24 kcal mol^{-1} (D_{3d}-III-C_{32}), and 78.24 kcal mol^{--1} (D_{3h}-V-C_{32}) by DFT calculations. The C_{32} fullerene cage comprises 6 hexagons and 12 pentagons. The researchers could not obtain negative frequency in the frequency calculations of the most stable structure. Figure 6 showed the optimized geometry (a), Mulliken charge distribution (b), MEP counter (c), and HOMO–LUMO plot (d) of the most stable isomer of the C_{32} fullerene cage.

As seen in Fig. 6, the Mulliken atomic charges on C in the C_{32} fullerene cage were divided into two groups. The Mulliken charges of the first group were 0.280 a.u. and 0.210 a.u. The charges were on twenty atoms and their color was green and its shades. The Mulliken charges of the second group were − 0.049 a.u., − 0.097 a.u., − 0.176 a.u., and − 0.503 a.u. The charges were on twelve atoms and their color was red and its shades. Lin et al. [45] reported that HOMO–LUMO energy gap of the lowest-energy of C_{32} fullerene cage with D_3 symmetry was obtained at 2.602 eV by means of B3LYP/6-31G(d,p) level. In the present study, the HOMO, LUMO, and HOMO–LUMO gap energies of the C_{32} fullerene cage were determined at − 6.624 eV, − 4.014 eV, and 2.610 eV for DFT/B3LYP level. The C_{70} and C_{60} fullerene cages were much larger and much more stable than the C_{32} fullerene cage. However, neutral C_{32} seems to have a much larger HOMO–LUMO gap value than those of C_{70} (1.3 eV) and C_{60} (1.6 eV) [45].

The EA of C_{32} was experimentally reported as ~ 2.8 eV [46]. In the present results (DFT/CAM-B3LYP level), EA_{ad} of C_{32} fullerene cage was obtained at 3.025 eV. Similarly, its EA_{vert} was calculated as 2.769 eV. IP and VDE values of C_{32} fullerene cage were found as 8.178 eV and 3.305 eV by DFT/CAM-B3LYP level (Table 1). The $\overline{\alpha}$ and the $\Delta\alpha$

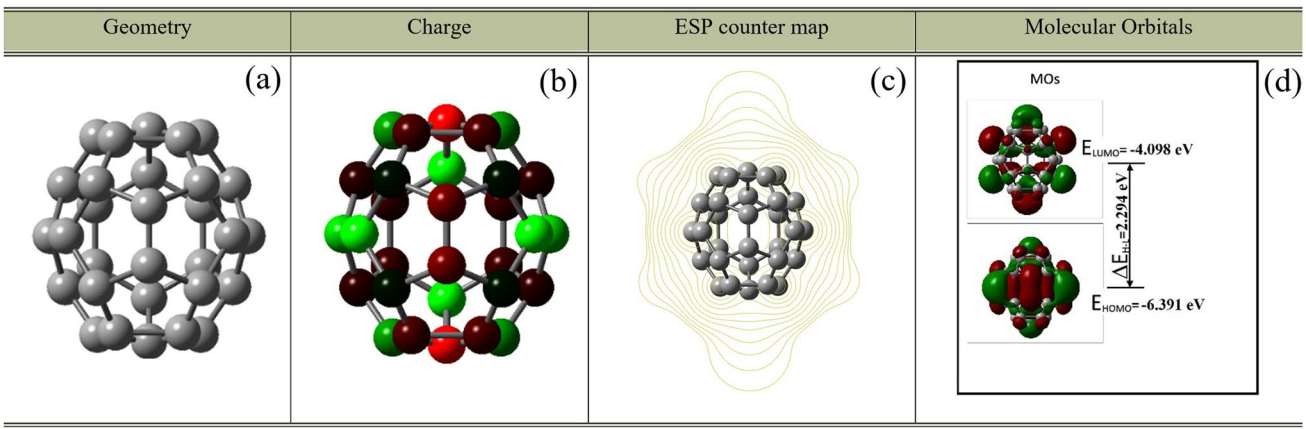

Fig. 5 Geometry, Mulliken charge, ESP counter map and HOMO, and LUMO plots of C30 fullerene cage

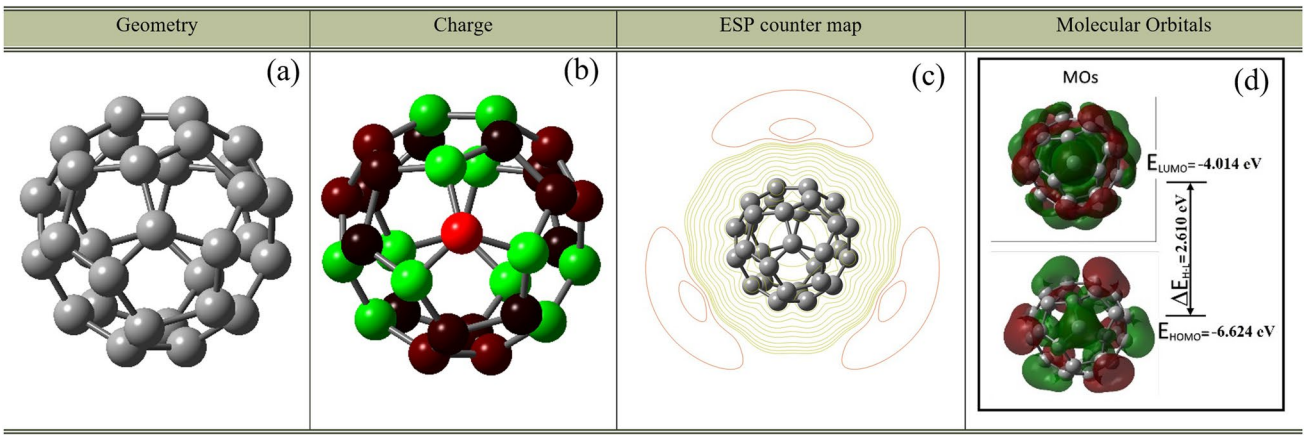

Fig. 6 Geometry, Mulliken charge, ESP counter map and HOMO, and LUMO plots of C32 fullerene cage

value of C_{30} fullerene cage were found 43.434×10^{-24} esu and 8.035×10^{-24} esu by DFT/CAM-B3LYP level (Table 2). All components of μ and β_0 values were calculated as zero.

There were six isomers for C_{34} fullerene cage. These isomers optimized by using the DFT/B3LYP level. Table S7 presents all calculation results such as optimization energy for each multiplicity, symmetry, and geometry of the C_{34} fullerene cages. These six isomers were determined according to their symmetry as follows: three C_2, two C_S, and one C_{3V}. In the DFT calculations, the most stable C_{34} fullerene cage was the C_2-V-C_{34} geometry with triplet multiplicity. Relative energies of other isomers with respect to the most stable geometry were determined at 13.661 kcal mol^{-1} (C_2-IV-C_{34}), 28.413 kcal mol^{-1} (C_s-II-C_{34}), 29.318 kcal mol^{-1} (C_S-III-C_{34}), 30.887 kcal mol^{-1} (C_{3V}-VI-C_{34}), and 73.936 kcal mol^{-1} (C_2-I-C_{34}) by DFT/B3LYP level. Figure 7 showed the optimized geometry (a), Mulliken charge distribution (b), MEP counter (c), and HOMO–LUMO plot (d) of the most stable isomer of the C_{34} fullerene cage.

The negative atomic charges on C in the C_{34} fullerene cage were determined at – 0.146 a.u., – 0.068 a.u., – 0.047 a.u., – 0.117 a.u., – 0.021 a.u., – 0.066 a.u., – 0.436 a.u., – 0.034 a.u., and – 0.278 a.u. (each charge was on two atoms.). These charges were shown in red color and its shades as seen in Fig. 7. The positive atomic charges on C in the C_{34} fullerene cage was found 0.222 a.u., 0.073 a.u., 0.261 a.u., 0.005 a.u., 0.163 a.u., 0.313 a.u., 0.064 a.u., and 0.112 a.u. (each charge is on two atoms.). These charges were shown in green color and its shades in the Fig. 7.

S. A. Halim et al. [47] predicted the electronic structure and stability of C_{34} and transition metal doped C_{34} derivative by using B3PW91/6-31G(d) level. In their study, the HOMO, LUMO, and HOMO–LUMO gap energies of the C_{34} fullerene cage were reported as—– 5.53 eV, 4.06 eV, and 1.47 eV, respectively. In the present study, the C_{34} fullerene cage had alpha and beta molecular orbitals because the most stable structure of C_{34} had triplet multiplicity. The HOMO energies of α and β orbitals were obtained as – 5.693 eV

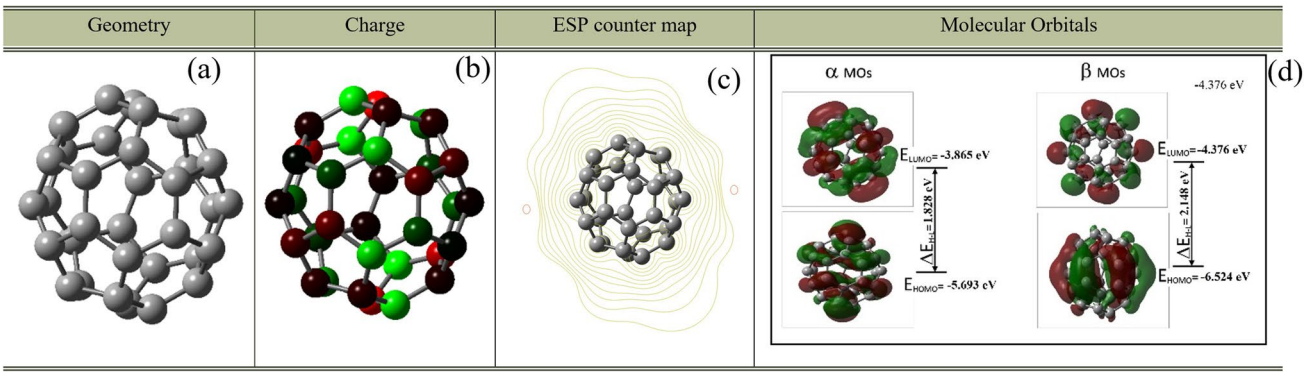

Fig. 7 Geometry, Mulliken charge, ESP counter map and HOMO, LUMO plots of C34 fullerene cage

and – 6.524 eV by DFT/B3LYP level. The LUMO energies of α and β orbitals were calculated as – 3.865 eV and – 4.376 eV. The HOMO–LUMO gap for α and β orbitals of C_{34} were found as 1.828 eV and 2.148 eV.

S. A. Halim et al. [47] reported the calculation results of the IP, EA, chemical hardness, electronegativity, chemical potential, electrophilicity of pure C_{34}, and transition metal-doped C_{34}. In that study, these data were calculated according to Koopman's theorem. It was addressed that the estimated IP value was 5.530 eV and the estimated EA value was 4.057 eV by the B3PW91/6-31G(d) level. In the present computational work, the IP, EA_{ad}, $EA_{vert,}$ and VDE values of C_{34} fullerene cage were obtained as 7.450 eV, 2.955 eV, 3.062 eV, and 3.163 eV, respectively (Table 1).

In the study by S.A. Halim et al. [47], all components of the μ, $\overline{\alpha}$, $\Delta\alpha$, and β_0 values of C_{34} fullerene cage were calculated and reported. In the same study, the $\overline{\alpha}$, the $\Delta\alpha$, μ, and β_0 values were also obtained by B3PW91/6-31G (d) level. In that study, 40.07×10^{-24} esu, 8.613×10^{-24} esu, 0.155 Debye, and 0.955×10^{-30} esu values were determined as the $\overline{\alpha}$, $\Delta\alpha$, μ, and β_0, respectively. In the present study, 46.062×10^{-24} esu, $8.103\times10^{--24}$ esu, 0.113 Debye, and 2.656×10^{-30} esu values were determined as the $\overline{\alpha}$, $\Delta\alpha$, μ, and β_0 by DFT/CAM-B3LYP level, respectively (Table 2).

C_{36} was one of the magic-number small fullerenes detected by mass spectroscopy in the very early days. C_{36} had 15 conventional fullerene isomers. Table S8 presents all calculation results such as optimization energy for each multiplicity, symmetry, and geometry of the C_{36} fullerene. D_{6h} and D_{2d} isomers contained a minimum number of adjacent pentagons. Therefore, they were candidates for the most stable structure. In the DFT calculations, it was revealed that the D_{6h}-XV-C_{36} fullerene cage with triplet multiplicity case was the most stable structure.

The symmetry and relative energies of other structures were determined as 1.800 kcal mol^{-1} for D_{2D}-XIV-C_{36}, 6.727 kcal mol^{-1} for C_2-XII-C_{36}, 7.173 kcal mol^{-1} for C_{2V}-IX-C_{36}, 13.17 kcal mol^{-1} for C_2-XI-C_{36}, 24.42 kcal mol^{-1} for C_S-VIII-C_{36}, 31.98 kcal mol^{-1} for D_{2D}-VI-C_{36}, 37.01 kcal mol^{-1} for C_1-VII-C_{36}, 40.61 kcal mol^{--1} for D_{3H}-XIII-C_{36}, 47.86 kcal mol^{-1} for C_2-X-C_{36}, 59.02 kcal mol^{-1} for C_1-III-C_{36}, 76.27 kcal mol^{-1} for C_S-IV-C_{36}, 84.41 kcal mol^{-1} for C_2-I-C_{36}, 90.66 kcal mol^{-1} for D_2-V-C_{36}, and 117.5 kcal mol^{-1} for D_2-II-C_{36}. Figure 8 showed the optimized geometry (a), Mulliken charge distribution (b), MEP counter (c), and HOMO–LUMO plot (d) of the most stable isomer of the C_{36} fullerene cage.

As seen in Fig. 8, the Mulliken atomic charges on C in the C_{36} fullerene cage were divided into three groups: $^{-}$0.057 a.u. (twelve atoms, red color), 0.052 a.u. (twelve atoms, green color), and 0.005 a.u. (twelve atoms, dark color). C_{36} fullerene cage had HOMO–LUMO gaps of 1.718 eV (alpha molecular orbital) and 1.744 eV (beta molecular orbital) which were calculated theoretically by DFT/B3LYP level. The HOMO–LUMO gap value (~ 1.7 eV) of C_{36} fullerene cage was determined close to those of C_{60} (1.6 eV) which was very stable and larger than itself.

Using photoelectron spectroscopy, the EA of the C_{36}^{-} anion in the gas phase was measured as 3.0 eV [46]. In theoretical study, EA and IP values of C_{36} fullerene cage with D_{6h} symmetry were calculated as 6.70 eV and 2.50 eV by B3LYP/6-31G(d) level [46]. In the present study, these properties were predicted as 7.335 eV (IP), 2.889 eV (EA_{ad}), 2.815 eV (EA_{vert}), and 2.962 eV (VDE) by DFT/CAM-B3LYP level (Table 1).

In the present study, the calculated the $\overline{\alpha}$ of C_{36} fullerene cage was obtained at $47.561\times10^{--24}$ esu by DFT/CAM-B3LYP level. Sabirov[29] et al. marked that the $\overline{\alpha}$ of C_{36} fullerene cage was 52.41×10^{-24} esu. The $\Delta\alpha$ of C_{36} fullerene cage was calculated as 0.909×10^{-24} esu by DFT/CAM-B3LYP level. Since C_{36} fullerene cage had a D_{6h} symmetry, all components of μ and β_0 values were found zero (Table 2).

There were 17 isomers of C_{38} fullerene cage. Table S9 presented all calculation results, such as optimization energy

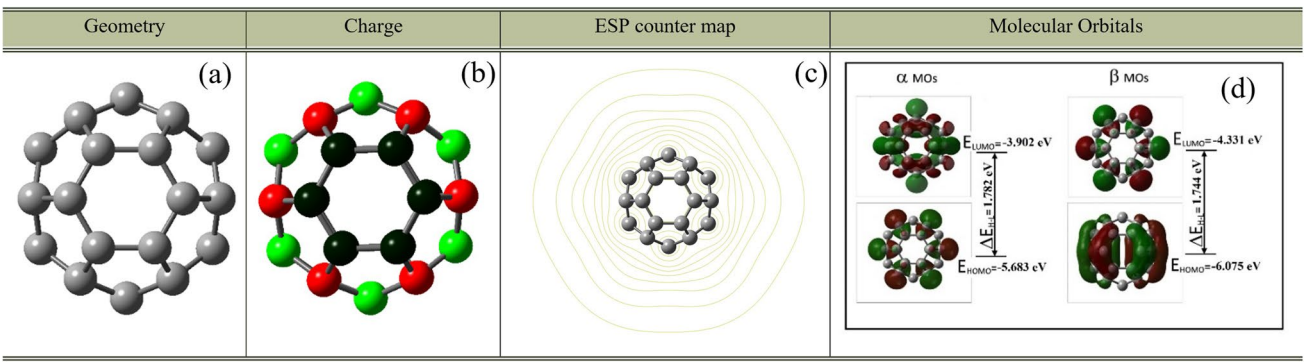

Fig. 8 Geometry, Mulliken charge, ESP counter map and HOMO, and LUMO plots of C36 fullerene cage

for each multiplicity, symmetry, and geometry of the C_{38} fullerene cage. The symmetries of these isomers were determined as five C_2 symmetry, seven C_1 symmetry, two C_{2V} symmetry, one C_{3V} symmetry, one D_3 symmetry, and one D_{3H} symmetry. In the DFT calculations, it was revealed that the C_2-XVII-C_{38} fullerene cage with singlet multiplicity case was the most stable structure. The relative energies of the other isomers were calculated as 18.78 kcal mol^{-1} for C_2-XIII-C_{38} isomer, 23.339 kcal mol^{-1} for C_2-X-C_{38} isomer, 54.390 kcal mol^{-1} for C_2-VI-C_{38} isomer, 102.601 kcal mol^{-1} for C_2-I-C_{38} isomer, 26.738 kcal mol^{-1} for C_1-XIV-C_{38} isomer, 38.048 kcal mol^{-1} for C_1-VIII-C_{38} isomer, 41.387 kcal mol^{-1} for C_1-V-C_{38} isomer, 45.983 kcal mol^{--1} for C_1-XI-C_{38} isomer, 62.956 kcal mol^{-1} for C_1-III-C_{38} isomer, 69.114 kcal mol^{-1} for C_1-VII-C_{38} isomer, 77.544 kcal mol^{-1} for C_1-IV-C_{38} isomer, 87.537 kcal mol^{-1} for C_{2V}-XII-C_{38} isomer, 50.486 kcal mol^{-1} for C_{2V}-XV-C_{38} isomer, 25.978 kcal mol^{-1} for C_{3V}-XVI-C_{38} isomer, 70.905 kcal mol^{-1} for D_3-IX-C_{38} isomer, and 131.451 kcal mol^{-1} for D_{3H}-II-C_{38} isomer. Figure 9 showed the optimized geometry (a), Mulliken charge distribution (b), MEP counter (c), and HOMO–LUMO plot (d) of the most stable isomer of the C38 fullerene cage.

The negative atomic charges on C in the C_{38} fullerene cage were determined at − 0.003 a.u., − 0.009 a.u., − 0.012 a.u., − 0.013 a.u., − 0.020 a.u., − 0.040 a.u., − 0.045 a.u., − 0.050 a.u., − 0.080 a.u., − 0.104 a.u., − 0.114 a.u., − 0.130 a.u., − 0.140 a.u., and − 0.16 a.u. (each charge is on two atoms.). These charges were shown in red and its shades in Fig. 9. The positive atomic charges on C in the C_{38} fullerene cage were found as 0.189 a.u., 0.083 a.u., 0.189 a.u., 0.247 a.u., and 0.218 a.u. (each charge is on two atoms.). These charges were shown in green and its shades in the Fig. 9. The researchers found HOMO, LUMO, and HOMO–LUMO gap values of C_2-XVII-C_{38} isomer in the C_{38} fullerene cages as − 5.832 eV, − 4.064 eV, and 1.768 eV by DFT/B3LYP level. The HOMO–LUMO gap of C_2-XVII-C_{38} isomer was close to those of C_{60} (1.6 eV).

In the present study, the IP, EA_{ad}, $EA_{vert,}$ and VDE properties of C_{38} fullerene cage were calculated at 7.335 eV, 2.889 eV, 2.815 eV, and 2.962 eV by DFT/CAM-B3LYP level respectively (Table 1). The obtained $\overline{\alpha}$ of C_{38} fullerene cage was at 49.958×10^{-24} esu by DFT/CAM-B3LYP level. The $\Delta\alpha$ of C_{38} fullerene cage was predicted as 5.917×10^{-24} esu by DFT/CAM-B3LYP level. μ was determined at 0.033 Debye, *the* β_0 values were found 0.289×10^{-30} esu by DFT calculations (Table 2).

Comparison of some properties

In conceptual DFT, Fukui functions could be employed as local descriptors to predict nucleophilic and electrophilic attacks. As seen in Figure S1, Fukui functions of C_N ($N = 20$, 24, 26, 28, 30, 32, 34, 36, and 38) fullerene cages are exhibited. Since the results from the Hirshfeld charge were reliable, the researchers calculated the Fukui function using the Hirshfeld charge. The nucleophilic region covered by the negative isosurfaces were the regions colored in blue and the electrophilic region covered by the positive isosurfaces were colored in green. As understood from the figure, both nucleophilic (blue areas in the figures) and electrophilic (green areas in the figures) regions were determined using the Hirshfeld charge of the carbon atoms in the fullerene. The images of the Fukui functions were obtained through the Multiwfn 3.8.8 program [48].

C_{60} was the most stable fullerene comprising 20 hexagons and 12 pentagons. Therefore, the focus of most of the experimental studies on fullerenes was C_{60} fullerene. In the present study, the researchers compared the HOMO LUMO values of the calculated fullerenes with the data of

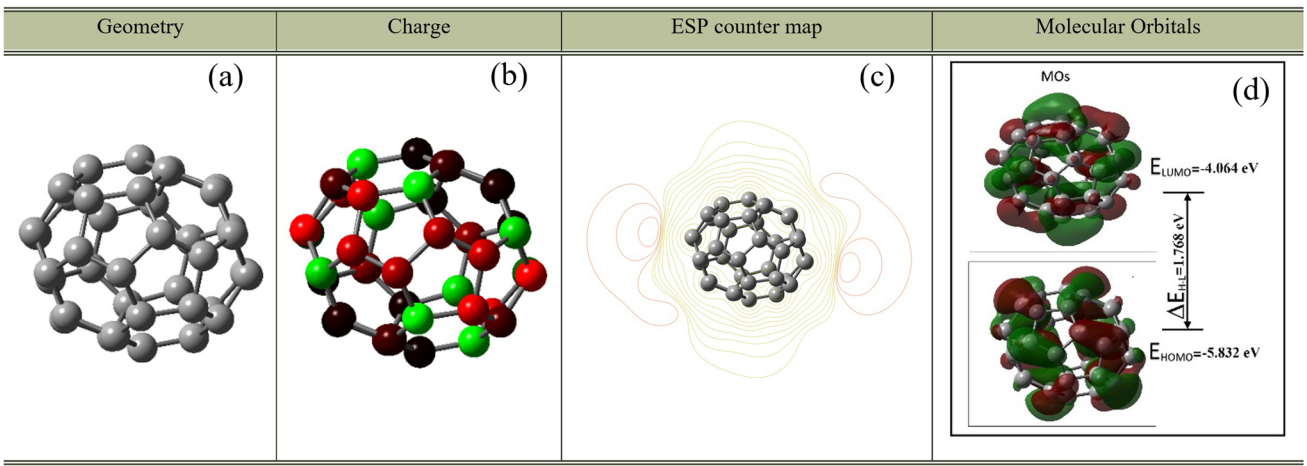

Fig. 9 Geometry, Mulliken charge, ESP counter map and HOMO, and LUMO plots of C38 fullerene cage

C_{60}. The HOMO–LUMO gaps of fullerenes calculated at the DFT B3LYP/6-311G (d,p) level have been proved to be useful in determining their stabilities. Fullerenes with HOMO–LUMO gap value greater than 1.3 eV had high stability. However, HOMO–LUMO gap value less than this value showed low stability. The studied fullerenes had HOMO–LUMO gap values greater than 1.3 eV (Table 3).

While the C_{26} and C_{28} fullerene cages were the most stable in quartet multiplicities, the C_{34} and C_{36} fullerene cages were the most stable in triplet multiplicities. As seen in Fig. 10, as the multiplicity increased, especially the LUMO value of the α orbitals increased. Therefore, the researchers compared the C_{60} values with fullerenes that were stable only at the singlet multiplicity. Since the C_{26}, C_{28}, C_{34}, and C_{36} fullerene cages were found to be stable at high multiplicities, the researchers did not make comparisons with the C_{60} data.

Wang et al. [49] calculated the HOMO, LUMO, and HOMO–LUMO gap values of C_{60} by B3LYP/6-311G(d,p) level. In their study, – 6.402 eV, – 3.658 eV, and 2.744 eV were predicted as HOMO, LUMO, and HOMO–LUMO gap of C_{60}, respectively. In the present study, the C_{32} fullerene cage had the highest HOMO–LUMO gap value (2.610 eV). C_{32} is a magic number carbon cluster that always gives very intense signals in gas phase experiments. In PES studies, it is stated that the neutral C_{32} molecule has a HOMO–LUMO gap comparable to C_{70} and C_{60} [46]. In the present study, the HOMO–LUMO value of the C_{32} fullerene cage closest to the HOMO–LUMO value of C_{60} was determined by DFT calculation.

Veries et al. reported that the IP of C_{60} was experimentally determined to 7.58 eV by using single-photon ionization [50]. As seen in Fig. 11, the sequence of magnitude of the IP values was determined as $C_{28} > C_{32} > C_{30} > C_{24} > C_{26} > C_{36} > C_{38} > C_{20}$. When evaluated on IP data, the researchers slightly overestimated the values of C_{24}, C_{28}, C_{30}, and C_{32} fullerene cages from the experimental value of C_{60}. The IP value of the other

Table 3 Comparison of HOMO–LUMO energies of studied neutral fullerenes with C60

Fullerenes	E_{HOMO} (eV)		E_{LUMO} (eV)		$\Delta E_{HOMO\text{-}LUMO}$ (eV)	
C20	– 5.442		– 3.506		1.936	
C24	– 6.050		– 4.221		1.829	
C26	– 6.135*	– 5.929 **	– 2.927*	– 4.314 **	3.208*	1.615**
C28	– 6.495*	– 6.606 **	– 2.293*	– 4.285 **	4.202*	2.321**
C30	– 6.391		– 4.098		2.293	
C32	– 6.624		– 4.014		2.610	
C34	– 5.693*	– 6.524 **	– 3.865*	– 4.376 **	1.828*	2.148**
C36	– 5.683*	– 6.075 **	– 3.902*	– 4.331 **	1.781*	1.744**
C38	– 5.832		– 4.064		1.768	
C60	– 6.402		– 3.658		2.744	

*Denotes the energy of the α molecular orbital

**Denotes the energy of the β molecular orbital

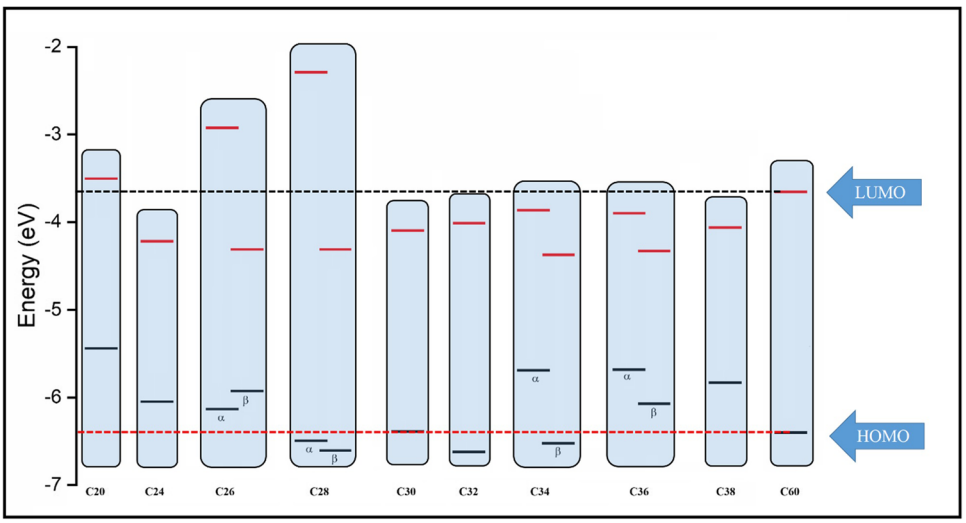

Fig. 10 HOMO, LUMO, and HOMO–LUMO gaps of the fullerene cages

fullerene cage were calculated slightly smaller than the C_{60} experimental data. The most accurate EA of C_{60} was determined as 2.6835 eV by the high-resolution photoelectron imaging [51]. When compared to the previous studies on fullerenes with the EA value of C_{60}, only the C_{20} and C_{26} fullerene cages values were calculated slightly small while the other fullerene cages were calculated slightly larger. Overall, it could be stated that the IP and EA values of the studied fullerenes were compatible with the C_{60} data.

Nabil et al. reported that the $\overline{\alpha}$ of C_{60} fullerene cage was calculated at 77.59×10^{-24} esu by CAM-B3LYP/6–31 + G(d,p) level [52]. Among the fullerenes studied, the smallest $\overline{\alpha}$ value was determined as 27.59×10^{-24} esu in C_{20} fullerene cage by DFT/CAM-B3LYP level. This value increased continuously for all fullerenes up to C_{38} fullerene. The $\overline{\alpha}$ value of C_{38} fullerene cage was determined as 49.95×10^{-24} esu by DFT/CAM-B3LYP level. Hyperpolarizability values of the C_{20}, C_{24}, C_{26}, C_{28}, C_{32}, and C_{36} fullerene cages with zero dipole moment were found zero. The other fullerenes had small dipole moments and small hyperpolarizability values.

Density of state (DOS) pictograms were obtained from Gaussian curves of unit height. DOS pictograms was obtained using the Mulliken population analysis results. DOS pictograms of fullerenes were obtained using the GaussSum 2.2 program [53]. The full width at half maximum (FWHM) at half height was used as 0.3 eV. The spectra of the state densities, which carry the orbital information of the molecules and emerge with the Gaussian type curves, were presented in Figure S2. The state density plots presented the population analysis per orbital. Figure S2 showed the DOS pictograms in the energy range − 20 to 0 eV. As seen in Figure S2, the DOS pictograms of the stable fullerenes in the singlet or high multiplicities were visualized. Total DOS pictograms in the singlet case and DOS pictograms of the α occupied and β virtual orbitals in the high multiplex case were created.

Conclusions

This study reported quantum chemical study of C_N ($N = 20$, 24, 26, 28, 30, 32, 34, 36, and 38) fullerene cages. More specifically, detailed structural, electronic, non-linear optical properties, Mulliken charge, density of state, and Fukui function analysis of these fullerenes were provided. In conclusion, the symmetries and multiplicities of the global minimum structure of these fullerene cages were found D_2 with singlet (C_{20}), D_6 with singlet (C_{24}), D_{3h} with quintet (C_{26}), T_d with quintet (C_{28}), C_{2v} with singlet (C_{30}), D_3 with singlet (C_{32}), C_2 with triplet (C_{34}), D_{6h} with triplet (C_{36}), and C_2 with singlet multiplicity (C_{38}). Hyperpolarizability values of the C_{20}, C_{24}, C_{26}, C_{28}, C_{32}, and C_{36} fullerene cages with zero dipole moment were found zero. The smallest mean polarizability value was determined in C_{20} fullerene cage. This value increased continuously for all fullerenes up to C_{38} fullerene. Succinctly, it could be stated that the ionization potential and electron affinity values of the studied fullerenes were compatible with the C_{60} data. The HOMO–LUMO value of the C_{32} fullerene cage closest to the HOMO–LUMO value of C_{60} was determined by DFT calculation.

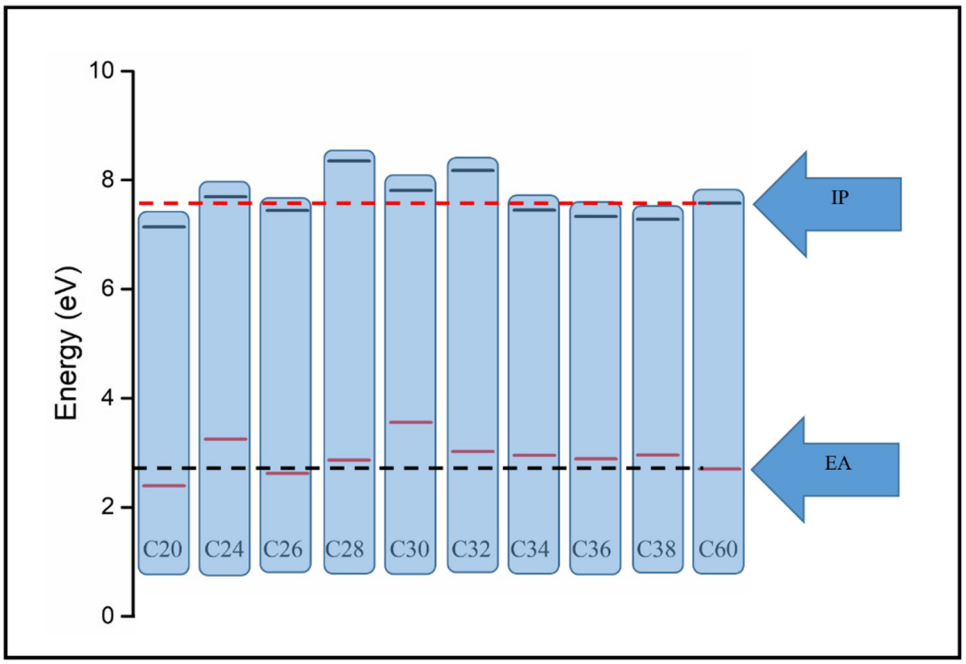

Fig. 11 Comparison of IP and EA of fullerenes with C60

Supplementary Information The online version contains supplementary material available at https://doi.org/10.1007/s00894-022-05348-9.

Acknowledgements The Quantum Chemical calculations reported in this paper were fully performed at Harran University High Performance Computing Center (Harran HPC resources).

Author contribution K. Soyarslan: investigation, writing – review & editing.

B. Ortatepe: resources writing – review & editing.

B. Yurduguzel: resources writing – review & editing.

M. T. Güllüoğlu: resources writing – review & editing.

Y. Erdogdu: investigation, writing – original draft, review & editing, supervision.

Declarations

Competing interests The authors declare no competing interests.

References

1. Kroto H (1997) Rev Mod Phys 69:703–722. https://doi.org/10.1103/RevModPhys.69.703
2. Dunk PW, Kaiser NK, Mulet-Gas M, Rodríguez-Fortea A, Poblet JM, Shinohara H, Hendrickson CL, Marshall AG, Kroto HW (2012) J Am Chem Soc 134:9380–9389. https://doi.org/10.1021/ja302398h
3. Chen Y-M, Shi J, Rui L, Guo Q-X (2009) J Mol Struct (Thoechem) 907:104–108. https://doi.org/10.1016/j.theochem.2009.04.038
4. Sun Q, Wang Q, Yu JZ, Ohno K, Kawazoe Y (2001) J Phys: Condens Matter 13:1931–1938. https://doi.org/10.1088/0953-8984/13/9/315
5. Paul D, Deb J, Sarkar U (2020) ChemistrySelect 5:6987–6999. https://doi.org/10.1002/slct.202001988
6. Alonso AM, Guldi DM, Paolucci F, Prato M (2007) Fullerenes: Multitask Components in Molecular Machinery Angew. Chem Int Ed 46:8120–8126. https://doi.org/10.1002/anie.200702725
7. Nierengarten JF et al (2000) Synthesis and electronic properties of donor-linked fullerenes towards photochemical molecular devices. Carbon 38:1587–1598. https://doi.org/10.1016/S0008-6223(99)00290-0
8. Kennedy RD, Ayzner AL, Wanger DD, Day CT, Halim M, Khan SI, Tolbert SH, Schwartz BJ, Rubin Y (2008) Self-assembling fullerenes for improved bulk-heterojunction photovoltaic devices. J Am Chem Soc 130:17290–17292. https://doi.org/10.1021/ja807627u
9. Golberg D, Bando Y, Stephan O, Kurashima K (1998) Octahedral boron nitride fullerenes formed by electron beam irradiation. Appl Phys Lett 73:2441. https://doi.org/10.1063/1.122475
10. Ying D, Yang Y, Yang Y, Fang H (2016) A novel fullerene-like B30N30 structure: Stability and electronic property. Carbon 102:273–278. https://doi.org/10.1016/j.carbon.2016.02.063
11. Alexandre SS, Mazzoni MSC, Chacham H (1999) Stability, geometry, and electronic structure of the boron nitride B36N36 fullerene. Appl Phys Lett 75:61. https://doi.org/10.1063/1.124277
12. Mocci P, Cardia R, Cappellini G (2019) A computational study on the electronic and optical properties of boron-nitride circumacenes. Phys Chem Chem Phys 21:16302–16309. https://doi.org/10.1039/C9CP01038F
13 Mocci P, Cardia R, Bosin A, Cappellini G (2020) Opto-electronic properties of BN-ring insertions in Circumacenes: the case of coronene and ovalene. J Phys Conf Ser. 1548:012028
14 Mocci P, Cardia R, Cappellini G (2019) A computational investigation on the electronic and optical properties of coronene and its boron-nitride and perfluorinated counterparts. J Phys Conf Ser 1226:012016
15. Frisch MJ, Trucks GW, Schlegel HB, Scuseria GE, Robb MA, Cheeseman JR, Scalmani G, Barone V, Petersson GA, Nakatsuji H, Li X, Caricato M, Marenich AV, Bloino J, Janesko BG, Gomperts R, Mennucci B, Hratchian HP, Ortiz JV, Izmaylov AF, Sonnenberg JL, Williams-Young D, Ding F, Lipparini F, Egidi F, Goings J, Peng B, Petrone A, Henderson T, Ranasinghe D, Zakrzewski VG, Gao J, Rega N, Zheng G, Liang W, Hada M, Ehara M, Toyota K, Fukuda R, Hasegawa J, Ishida M, Nakajima T, Honda Y, Kitao O, Nakai H, Vreven T, Throssell K, Montgomery JA, Peralta JJE, Ogliaro F, Bearpark MJ, Heyd JJ, Brothers EN, Kudin KN, Staroverov VN, Keith TA, Kobayashi R, Normand J, Raghavachari K, Rendell AP, Burant JC, Iyengar SS, Tomasi J, Cossi M, Millam JM, Klene M, Adamo C, Cammi R, Ochterski JW, Martin RL, Morokuma K, Farkas O, Foresman JB, Fox DJ (2016) Gaussian 16, Revision B.01. Gaussian Inc, Wallingford CT
16. Becke AD (1993) J Chem Phys 98:5648–5653
17. Lee C, Yang W, Parr RG (1988) Phys Rev B 37:785–789
18. Yanai T, Tew DP, Handy NC (2004) Chem Phys Lett 393:51–57. https://doi.org/10.1016/j.cplett.2004.06.011
19. Krishnan R, Binkley JS, Seeger R, Pople JA (1980) J Chem Phys 72:650–654. https://doi.org/10.1063/1.438955
20. Mitsuho Yoshida, Fullerene Structure Library (n.d.) https://nanotube.msu.edu/fullerene/fullerene-isomers.html. Accessed 15 Sept 2021
21. Alparone A (2013) Response electric properties of α-helix polyglycines: a CAM-B3LYP DFT investigation Chem. Phys Lett 536:88–92. https://doi.org/10.1016/j.cplett.2013.01.062
22 Peach MJG, Helgaker T, Sałek P, Keal TW, Lutnæs OB, Tozer DJ, Handy NC (2006) Assessment of a Coulomb-attenuated exchange–correlation energy functional. Phys. Chem. Chem Phys 8:558–562. https://doi.org/10.1039/B511865D
23. Kobayashi R, Amos RD (2006) The application of CAM-B3LYP to the charge-transfer band problem of the zincbacteriochlorin–bacteriochlorin complex. Chem Phys Lett 420:106–109. https://doi.org/10.1016/j.cplett.2005.12.040
24. Jacquemin D, Perpète EA, Medved M, Scalmani G, Frisch MJ, Kobayashi R, Adamo C (2007) First hyperpolarizability of polymethineimine with long-range corrected functional. J Chem Phys 126:191108. https://doi.org/10.1063/1.2741246
25. Limacher A, Mikkelsen KV, Lüthi HP (2009) On the accurate calculation of polarizabilities and second hyperpolarizabilities of polyacetylene oligomer chains using the CAM-B3LYP density functional. J Chem Phys 130:194114. https://doi.org/10.1063/1.3139023
26. Shakerzadeh E, Tahmasebi E, Biglari Z (2016) A quantum chemical study on the remarkable nonlinear optical and electronic characteristics of boron nitride nanoclusters by complexation via lithium atom. J Mol Liq 221:443–451. https://doi.org/10.1016/j.molliq.2016.05.090
27. Erdogdu Y, Erkoc S (2012) Jnl of Comp & Theo. NANO 9:837–850. https://doi.org/10.1166/jctn.2012.2105
28. Subashchandrabose S, Saleem H, Erdogdu Y, Dereli Ö, Thanikachalam V, Jayabharathi J (2012) Spectrochim Acta Part A Mol Biomol Spectrosc 86:231–241. https://doi.org/10.1016/j.saa.2011.10.029
29. Atilgan A, Yurdakul Ş, Erdogdu Y, Güllüoğlu MT (2018) J Mol Struct 1161:55–65. https://doi.org/10.1016/j.molstruc.2018.01.080

30. Rad AS, Ayub K (2018) Mater Res Bull 97:399–404. https://doi.org/10.1016/j.materresbull.2017.09.036
31. Wang Z, Lian K, Pan S, Fan X (2005) J Comput Chem 26:1279–1283. https://doi.org/10.1002/jcc.20268
32. Prinzbach H, Weiler A, Landenberger P, Wahl F, Wörth J, Scott LT, Gelmont M, Olevano D, Issendorff BV (2000) Nature 407:60–63. https://doi.org/10.1038/35024037
33. Rad AS, Ayub K (2019) Appl Phys A 125:430. https://doi.org/10.1007/s00339-019-2721-7
34. Yang S, Pettiette CL, Conceicao J, Cheshnovsky O, R E Smalley (1987) 139:233–238. https://doi.org/10.1016/0009-2614(87)80548-1
35. Wang LS, Conceicao J, Jin CM, Smalley RE (1991) Chem Phys Lett 182:5. https://doi.org/10.1016/0009-2614(91)80094-E
36. Wang X-B, Ding C-F, Wang L-S (1999) J Chem Phys 110:8217–8220. https://doi.org/10.1063/1.478732
37. Jensen F, Koch H (1998) J Chem Phys 108:3213–3217. https://doi.org/10.1063/1.475716
38. Heidari Nezhad Janjanpour M, Vakili M, Daneshmehr S, Jalalierad K, Alipour F (2018) Chem Rev Lett 1. https://doi.org/10.22034/crl.2018.85215.
39. Kosar N, Tahir H, Ayub K, Mahmood T (2021) J Mol Graph Model 105:107867. https://doi.org/10.1016/j.jmgm.2021.107867
40. Balevičius LM, Stumbrys E, Tamulis A (1997) Fullerene Sci Technol 5:85–96. https://doi.org/10.1080/15363839708011974
41. An J, Gan LH, Zhao JQ, Li R (2010) The Journal of Chemical Physics 132:154304
42. Adjizian J-J, Vlandas A, Rio J, Charlier J-C, Ewels CP (2016) Phil Trans R Soc A 374:20150323. https://doi.org/10.1098/rsta.2015.0323
43 Muñoz-Castro A, Bruce King R (2017) J Comput Chem 38:44–50. https://doi.org/10.1002/jcc.24518
44. Sabirov DSh, Bulgakov RG (2010) Jetp Lett 92:662–665. https://doi.org/10.1134/S0021364010220054
45. Lin J, Hu J, Zhang J-R, Wang S-Y, Ma Y, Song X-N (2019) Spectrochim Acta Part A Mol Biomol Spectrosc 212:180–187. https://doi.org/10.1016/j.saa.2018.12.043
46. Lu X, Chen Z (2005) Chem Rev 105:3643–3696. https://doi.org/10.1021/cr030093d
47. Halim SA (2018) Int J Nano Dimens 9(4):421–434
48. Lu T, Chen F (2012) Multiwfn: A multifunctional wavefunction analyzer. J Comput Chem 33:580–592. https://doi.org/10.1002/jcc.22885
49. Wang H, He Y, Li Y, Su H (2012) J Phys Chem A 116:255–262. https://doi.org/10.1021/jp208520v
50. de Vries J, Steger H, Kamke B, Menzel C, Weisser B, Kamke W, Hertel IV (n.d.) Chem Phys Lett. 188 4
51. Huang D-L, Dau PD, Liu H-T, Wang L-S (2014) J Chem Phys 140:224315. https://doi.org/10.1063/1.4881421
52. Omri N, Bu Y (2021) J Phys Chem A 125:106–114. https://doi.org/10.1021/acs.jpca.0c08533
53 Oboyle NM, Tenderholt AL, Langner KM (2008) J Comput Chem 29:839–845. https://doi.org/10.1002/jcc.20823